An efficient ergodic simulation of multivariate stochastic processes with spectral representation

Quanshun Ding *, Ledong Zhu, Haifan Xiang

State Key Lab for Disaster Reduction in Civil Engineering, Tongji University, Shanghai 200092, China

ARTICLE INFO

ABSTRACT

A simulation formula to generate stationary multivariate stochastic processes is derived from the Fourier–Stieltjes integral of spectral representation. It is proved that the proposed algorithm generates ergodic sample functions in the mean value and in the correlation when the sample length is equal to one period (the generated sample functions are periodic). The algorithm is very efficient computationally since it takes advantage of the fast Fourier transform technique. The simulation of longitudinal wind velocity fluctuations and the simulation of longitudinal and vertical wind fluctuating components on a bridge deck are performed. It has been noted that there are good agreements between the temporal and target auto-/cross-correlation functions of simulated wind velocities.

© 2011 Published by Elsevier Ltd

1. Introduction

The time-domain approach based on Monte Carlo methodology appears be very suitable for the solution of certain problems in stochastic mechanics involving nonlinearity, stochastic stability, parametric excitation, etc. One of the most important steps of a Monte Carlo time-domain simulation is to generate the sample functions of the stochastic processes, fields, or waves in the problem.

Although there are now many methods available to simulate such multivariate stochastic fields [1], spectral representation methods appear to be most widely used because of their versatility and robustness, and they are discussed in this paper. The basic method for analyzing a one-dimensional, one-variate Gaussian process appeared in the 1950s. To our knowledge, Shinozuka [2,3] was the foremost person who applied the spectral representation method for simulation purposes including multidimensional, multivariate, and nonstationary cases. Yang [4] showed that the fast Fourier transform (FFT) technique could be used to improve the computational efficiency of the spectral representation algorithm dramatically, and proposed a formula to simulate random envelope processes. Shinozuka [5] extended the application of the FFT technique to multidimensional cases. In 1996, Deodatis [6] further extended the spectral representation method to generate ergodic sample functions of multivariate stochastic processes.

Moreover, several review papers on the subject of simulation using the spectral representation method were written by Shinozuka [7], and Shinozuka and Deodatis [8].

The spectral representation method has been further developed in the actual application of simulation of wind fields, earthquake waves, etc. [9–17]. Through introducing an explicit form of the Cholesky decomposition of a special power spectrum density (PSD) matrix, Yang [13] and Cao and Xiang [14] greatly improved the efficiency of Shinozuka's and Deodatis' methods respectively for simulating the wind velocity along the horizontal axis of bridge decks. Although the Deodatis method can produce unconditionally stable and satisfactory results, it is computationally expensive due to the repetitive decomposition of the power density matrix when a number of random processes are to be simulated. Meanwhile, the improvement to the Deodatis method made by Cao and Xiang [14] has a severe restriction on the simulated stochastic field: both the auto-spectral power spectra at simulated points and their spacing must be identical.

In this paper, an efficient simulation formula to generate stationary multivariate stochastic processes is derived from the Fourier–Stieltjes integral of spectral representation. The proposed algorithm generates ergodic sample functions in the mean value and in the correlation when the sample length is equal to one period. The algorithm is very efficient computationally since it takes advantage of the fast Fourier transform technique. Moreover, the simulation of longitudinal wind velocity fluctuations and the simulation of longitudinal and vertical wind fluctuating components on a horizontal bridge deck are performed in order to demonstrate the capability and efficiency of the proposed algorithm.

---

* Corresponding author.
E-mail address: qsding@tongji.edu.cn (Q. Ding).

2. Simulation formula

Consider a set of n stationary stochastic processes $\{X_j^0(t)\}$ ($j = 1, 2, \ldots, n$) with their mean values being zero, where the superscript 0 denotes the target function. The cross-correlation matrix $\mathbf{R}^0(\tau)$ is given by

$$\mathbf{R}^0(\tau) = \begin{bmatrix} R_{11}^0(\tau) & R_{12}^0(\tau) & \cdots & R_{1n}^0(\tau) \\ R_{21}^0(\tau) & R_{22}^0(\tau) & \cdots & R_{2n}^0(\tau) \\ \vdots & \vdots & \ddots & \vdots \\ R_{n1}^0(\tau) & R_{n2}^0(\tau) & \cdots & R_{nn}^0(\tau) \end{bmatrix} \tag{1}$$

and the two-sided cross-spectral density matrix $\mathbf{S}^0(\omega)$ is given by

$$\mathbf{S}^0(\omega) = \begin{bmatrix} S_{11}^0(\omega) & S_{12}^0(\omega) & \cdots & S_{1n}^0(\omega) \\ S_{21}^0(\omega) & S_{22}^0(\omega) & \cdots & S_{2n}^0(\omega) \\ \vdots & \vdots & \ddots & \vdots \\ S_{n1}^0(\omega) & S_{n2}^0(\omega) & \cdots & S_{nn}^0(\omega) \end{bmatrix}. \tag{2}$$

The elements of the cross-correlation matrix are related to the corresponding elements of the cross-spectral density matrix through the Wiener–Khintchine transformation

$$S_{jk}^0(\omega) = \frac{1}{2\pi} \int_{-\infty}^{\infty} R_{jk}^0(\tau) e^{-i\omega\tau} d\tau, \quad j, k = 1, 2, \ldots, n \tag{3a}$$

$$R_{jk}^0(\tau) = \int_{-\infty}^{\infty} S_{jk}^0(\omega) e^{i\omega\tau} d\omega, \quad j, k = 1, 2, \ldots, n. \tag{3b}$$

For actual stochastic processes, the auto-spectral density function is a real and nonnegative function of ω and the cross-spectral density function is a generally complex function of ω. The following relations are valid:

$$\begin{aligned} S_{jj}^0(\omega) &= S_{jj}^0(-\omega), \qquad S_{jk}^0(\omega) = S_{jk}^{0*}(-\omega), \\ S_{jk}^0(\omega) &= S_{kj}^{0*}(\omega) \end{aligned}, \tag{4}$$

where $j, k = 1, 2, \ldots, n$, and the asterisk denotes the complex conjugate. Thus the cross-spectral density matrix $\mathbf{S}^0(\omega)$ is Hermitian. When the simulated stochastic processes are independent, $\mathbf{S}^0(\omega)$ is usually nonsingular. The matrix $\mathbf{S}^0(\omega)$ can be decomposed into the following format:

$$\mathbf{S}^0(\omega) = \mathbf{H}^*(\omega)\mathbf{H}^T(\omega) \tag{5}$$

$$\mathbf{H}(\omega) = \begin{bmatrix} H_{11}(\omega) & 0 & \cdots & 0 \\ H_{21}(\omega) & H_{22}(\omega) & \cdots & 0 \\ \cdots & \cdots & \cdots & \cdots \\ H_{n1}(\omega) & H_{n2}(\omega) & \cdots & H_{nn}(\omega) \end{bmatrix},$$

where the superscript T denotes the transpose of a matrix; $\mathbf{H}(\omega)$ is the lower triangular matrix. This decomposition can be performed using Cholesky's method. In general, the diagonal and off-diagonal elements of the lower triangular matrix are complex functions of ω. There are the following relations for the elements of matrix $\mathbf{H}(\omega)$:

$$H_{jk}(\omega) = H_{jk}^*(-\omega), \quad j, k = 1, 2, \ldots, n, j \geq k. \tag{6}$$

If the elements $H_{jk}(\omega)$ are written in polar form as

$$H_{jk}(\omega) = |H_{jk}(\omega)| e^{i\theta_{jk}(\omega)}, \quad j, k = 1, 2, \ldots, n, \tag{7}$$

where $\theta_{jk}(\omega)$ is the complex angle of $H_{jk}(\omega)$ and is given by

$$\theta_{jk}(\omega) = \tan^{-1} \left\{ \frac{\text{Im}\,[H_{jk}(\omega)]}{\text{Re}\,[H_{jk}(\omega)]} \right\} \tag{8}$$

with Im[ ] and Re[ ] being the imaginary and real parts of the complex function in parentheses, respectively, then Eq. (6) is written equivalently as

$$|H_{jk}(\omega)| = |H_{jk}(-\omega)|, \quad j, k = 1, 2, \ldots, n, j \geq k \tag{9a}$$

$$\theta_{jk}(\omega) = -\theta_{jk}(-\omega), \quad j, k = 1, 2, \ldots, n, j \geq k. \tag{9b}$$

Based on the spectral analysis, each of the n stochastic processes may be expressed as a Fourier–Stieltjes integral over a random Fourier increment [18]:

$$X_j(t) = \int_{-\infty}^{\infty} e^{i\omega t} dZ_j(\omega), \quad j = 1, 2, \ldots, n. \tag{10}$$

The random increment must satisfy the following orthogonality conditions:

$$E[dZ_j(\omega)] = 0$$
$$E[dZ_j^*(\omega)dZ_k(\omega')] = 0, \quad \omega \neq \omega' \tag{11}$$
$$E[dZ_j^*(\omega)dZ_k(\omega)] = S_{jk}(\omega)d\omega,$$

where $E[\cdot]$ is the mathematical expectation. It is noted that the two Fourier increments $dZ_j(\omega)$ and $dZ_k(\omega')$ are statistically correlated only when $\omega = \omega'$. When the simulated processes $X_j(t)$ ($j = 1, 2, \ldots, n$) are real, the relation $dZ_j(-\omega) = dZ_j^*(\omega)$ is also required.

Eq. (10) can be rewritten as

$$\begin{aligned} X_j(t) &= \int_0^{\infty} e^{i\omega t} dZ_j(\omega) + \int_{-\infty}^0 e^{i\omega t} dZ_j(\omega) \\ &= \int_0^{\infty} e^{i\omega t} dZ_j(\omega) + \int_0^{\infty} e^{-i\omega t} dZ_j(-\omega). \end{aligned} \tag{12}$$

Introducing the relations $e^{-i\omega t} = (e^{i\omega t})^*$ and $dZ_j(-\omega) = dZ_j^*(\omega)$, then

$$\begin{aligned} X_j(t) &= \int_0^{\infty} e^{i\omega t} dZ_j(\omega) + \int_0^{\infty} [e^{i\omega t} dZ_j(\omega)]^* \\ &= 2\text{Re}\left[\int_0^{\infty} e^{i\omega t} dZ_j(\omega)\right]. \end{aligned} \tag{13}$$

The discrete approximation to the random Fourier increment in Eq. (13) can be constructed in various ways. In the proposed scheme, the following approximate expression is utilized:

$$dZ_j(\omega)|_{\omega=\omega_l} \approx \Delta Z_j(\omega_l) = \sum_{m=1}^n H_{jm}(\omega_l) e^{i\phi_{ml}} \sqrt{\Delta\omega} \tag{14}$$

$$\omega_l = l\Delta\omega + \Delta\omega/2, \quad l = 0, \ldots, N-1, \tag{15}$$

where N is a sufficiently large number; $\Delta\omega = \omega_{up}/N$ is the frequency increment, ω_{up} is the upper cutoff frequency, with the condition that, when $\omega > \omega_{up}$, the value of $\mathbf{S}^0(\omega)$ is trivial; ϕ_{ml} are sequences of independent random phase angles, uniformly distributed over the interval $[0, 2\pi]$. Meanwhile, the exponential term in Eq. (13) is discretized using the double-indexing frequency [6]

$$e^{i\omega t}|_{\omega=\omega_{ml}} = e^{i\omega_{ml}t}, \qquad \omega_{ml} = l\Delta\omega + \frac{m}{n}\Delta\omega,$$
$$l = 0, 1, \ldots, N-1. \tag{16}$$

Inserting Eqs. (14), (16) and (7) into Eq. (13), then

$$\begin{aligned} X_j(t) &= \int_{-\infty}^{\infty} e^{i\omega t} dZ_j(\omega) \\ &\approx 2\text{Re}\left[\sum_{l=0}^{N-1}\sum_{m=1}^n H_{jm}(\omega_l) e^{i(\omega_{ml}t+\phi_{ml})} \sqrt{\Delta\omega}\right] \end{aligned}$$

$$= 2\sqrt{\Delta\omega}\,\mathrm{Re}\left\{\sum_{l=0}^{N-1}\sum_{m=1}^{n}|H_{jm}(\omega_l)|e^{i[\omega_{ml}t+\phi_{ml}+\theta_{jm}(\omega_l)]}\right\}$$

$$= 2\sqrt{\Delta\omega}\sum_{l=0}^{N-1}\sum_{m=1}^{n}|H_{jm}(\omega_l)|\cos[\omega_{ml}t+\phi_{ml}+\theta_{jm}(\omega_l)]. \quad (17)$$

It has been noted that the proposed simulation formula derived from the Fourier–Stieltjes integral is similar in form to the Deodatis method [6]. A main difference is that the double-indexing frequency is used in the Cholesky decomposition of the PSD matrix $\mathbf{S}^0(\omega)$ in the Deodatis method, so the decomposition has to be performed separately for every frequency ω_{ml}. However, the proposed simulation scheme drastically reduces the computation requirements for Cholesky decomposition. The ergodicity of the proposed simulation processes will be proved in the following.

The period of the generated sample functions expressed by Eq. (17) is

$$T_0 = \frac{2\pi n}{\Delta\omega} = \frac{2\pi nN}{\omega_{up}}. \quad (18)$$

In order to avoid aliasing according to the sampling theorem, the time step Δt has to obey the condition

$$\Delta t \le \frac{2\pi}{2\omega_{up}}. \quad (19)$$

It is obvious that the ensemble average $E[X_j(t)]$ $(j = 1, 2, \ldots, n)$ is zero. And the ensemble auto-/cross-correlation function $R_{jk}(\tau)$ with $j \ge k$ is

$$R_{jk}(\tau) = E[X_j(t)X_k(t+\tau)]$$
$$= 4\Delta\omega\sum_{m_1=1}^{n}\sum_{m_2=1}^{n}\sum_{l_1=0}^{N-1}\sum_{l_2=0}^{N-1}|H_{jm_1}(\omega_{l_1})|\,|H_{km_2}(\omega_{l_2})|$$
$$\times E\{\cos[\omega_{m_1l_1}t+\phi_{m_1l_1}+\theta_{jm_1}(\omega_{l_1})]\cdot\cos[\omega_{m_2l_2}(t+\tau)$$
$$+\phi_{m_2l_2}+\theta_{km_2}(\omega_{l_2})]\}. \quad (20)$$

Since the ϕs are independent random variables distributed uniformly over the interval $[0, 2\pi]$, the expected value in Eq. (20) is equal to zero when $m_1 \ne m_2$ or $l_1 \ne l_2$, so

$$R_{jk}(\tau) = 2\Delta\omega\sum_{m=1}^{n}\sum_{l=0}^{N-1}|H_{jm}(\omega_l)|\,|H_{km}(\omega_l)|\cdot E\{\cos[2\omega_{ml}t$$
$$+\omega_{ml}\tau+2\phi_{ml}+\theta_{jm}(\omega_l)+\theta_{km}(\omega_l)]$$
$$+\cos[\omega_{ml}\tau-\theta_{jm}(\omega_l)+\theta_{km}(\omega_l)]\}$$
$$= 2\Delta\omega\sum_{m=1}^{n}\sum_{l=0}^{N-1}|H_{jm}(\omega_l)|\,|H_{km}(\omega_l)|\cos[\omega_{ml}\tau-\theta_{jm}(\omega_l)$$
$$+\theta_{km}(\omega_l)]. \quad (21)$$

Since the power spectral density $S_{jk}(\omega)$ is assumed to be zero for $|\omega| > \omega_{up}$, the expression $R_{jk}(\tau)$ in Eq. (21) becomes the following in the limit as $\Delta\omega \to 0$ and $N \to \infty$:

$$R_{jk}(\tau) = \int_{-\infty}^{\infty}\sum_{m=1}^{n}|H_{jm}(\omega)|\,|H_{km}(\omega)|e^{i[\omega\tau-\theta_{jm}(\omega)+\theta_{km}(\omega)]}\mathrm{d}\omega$$

$$= \int_{-\infty}^{\infty}\sum_{m=1}^{n}H_{jm}^{*}(\omega)H_{km}(\omega)e^{i\omega\tau}\mathrm{d}\omega. \quad (22)$$

Using the decomposition shown in Eq. (5),

$$R_{jk}(\tau) = \int_{-\infty}^{\infty}S_{jk}^0(\omega)e^{i\omega\tau}\mathrm{d}\omega = R_{jk}^0(\tau). \quad (23)$$

Thus, the above expression shows that the ensemble auto-/cross-correlation function given by Eq. (17) will approach the target as $\Delta\omega \to 0$ and $N \to \infty$.

3. Ergodicity of simulated processes

It will be shown that an important property of the proposed simulated stochastic process is that it is ergodic in the mean value and in correlation. That is to say, the temporal mean value and temporal auto-/cross-correlation function of any sample function $X_j^{(i)}(t)$ $(j = 1, 2, \ldots, n)$ given by Eq. (17) are identical to the corresponding ensemble parts when the sample length is equal to T_0 (one period).

Since the sample function $X_j^{(i)}(t)$ $(j = 1, 2, \ldots, n)$ with a summation of cosine functions is a periodic function of t with a period of T_0, it is obvious that the temporal average is

$$\left\langle X_j^{(i)}(t)\right\rangle_T = 0 = E[X_j(t)], \quad \text{when } T = T_0. \quad (24)$$

The temporal auto-/cross-correlation function $R_{jk}^{(i)}(\tau)$ $(j, k = 1, 2, \ldots, n)$ of any sample function over a time interval equal to T is

$$R_{jk}^{(i)}(\tau) = \left\langle X_j^{(i)}(t)X_k^{(i)}(t+\tau)\right\rangle_T = \frac{1}{T}\int_0^T X_j^{(i)}(t)X_k^{(i)}(t+\tau)\mathrm{d}t$$

$$= \frac{1}{T}\int_0^T 4\Delta\omega\sum_{m_1=1}^{n}\sum_{m_2=1}^{n}\sum_{l_1=0}^{N-1}\sum_{l_2=0}^{N-1}|H_{jm_1}(\omega_{l_1})|\,|H_{km_2}(\omega_{l_2})|$$
$$\times \cos[\omega_{m_1l_1}t+\phi_{m_1l_1}+\theta_{jm_1}(\omega_{l_1})]\cdot\cos[\omega_{m_2l_2}(t+\tau)$$
$$+\phi_{m_2l_2}+\theta_{km_2}(\omega_{l_2})]\mathrm{d}t$$

$$= \frac{2}{T}\Delta\omega\sum_{m_1=1}^{n}\sum_{m_2=1}^{n}\sum_{l_1=0}^{N-1}\sum_{l_2=0}^{N-1}|H_{jm_1}(\omega_{l_1})|\,|H_{km_2}(\omega_{l_2})|$$

$$\times\left\{\int_0^T\cos[(\omega_{m_1l_1}+\omega_{m_2l_2})t+\omega_{m_2l_2}\tau+\phi_{m_1l_1}+\phi_{m_2l_2}\right.$$
$$+\theta_{jm_1}(\omega_{l_1})+\theta_{km_2}(\omega_{l_2})]\mathrm{d}t+\int_0^T\cos[(\omega_{m_2l_2}-\omega_{m_1l_1})t$$
$$\left.+\omega_{m_2l_2}\tau-\phi_{m_1l_1}+\phi_{m_2l_2}-\theta_{jm_1}(\omega_{l_1})+\theta_{km_2}(\omega_{l_2})]\mathrm{d}t\right\}. \quad (25)$$

Due to the periodicity of the terms $\cos[(\omega_{m_1l_1}+\omega_{m_2l_2})t]$, for any combination of l_1, l_2, m_1, m_2, when $T = T_0 = \frac{2\pi n}{\Delta\omega}$,

$$\int_0^T\cos[(\omega_{m_1l_1}+\omega_{m_2l_2})t]\mathrm{d}t = 0. \quad (26)$$

Similarly, the integral terms $\int_0^T\cos[(\omega_{m_2l_2}-\omega_{m_1l_1})t]\mathrm{d}t$ are also equal to zero for the case $m_1 \ne m_2$ or $l_1 \ne l_2$, when $T = T_0$. Therefore, the temporal auto-/cross-correlation function for $T = T_0$ becomes

$$R_{jk}^{(i)}(\tau) = \frac{2}{T_0}\Delta\omega\sum_{m=1}^{n}\sum_{l=0}^{N-1}|H_{jm}(\omega_l)|\,|H_{km}(\omega_l)|$$

$$\times\int_0^{T_0}\cos[\omega_{ml}\tau-\theta_{jm}(\omega_l)+\theta_{km}(\omega_l)]\mathrm{d}t$$

$$= 2\Delta\omega\sum_{m=1}^{n}\sum_{l=0}^{N-1}|H_{jm}(\omega_l)|\,|H_{km}(\omega_l)|$$

$$\times\cos[\omega_{ml}\tau-\theta_{jm}(\omega_l)+\theta_{km}(\omega_l)]. \quad (27)$$

Comparing Eq. (27) with Eq. (21), the following relation can be found:

$$R_{jk}^{(i)}(\tau) = \left\langle X_j^{(i)}(t)X_k^{(i)}(t+\tau)\right\rangle_T$$
$$= E[X_j(t)X_k(t+\tau)], \quad j, k = 1, 2, \ldots, n. \quad (28)$$

Eqs. (24) and (28) show that every sample function given by Eq. (17) is ergodic in the mean value and in correlation when the sample length is equal to the period T_0.

4. Application of the fast Fourier transform technique

The cost of digitally generating sample functions of the simulated stochastic processes can be drastically reduced using the FFT technique [4,6]. To take advantage of the FFT technique, Eq. (17) is rewritten explicitly in the following form:

$$X_j(p\Delta t) = \mathrm{Re}\left\{\sum_{m=1}^{j} C_{jm}(q\Delta t) \exp\left[i\left(\frac{m\Delta\omega}{n}\right)(p\Delta t)\right]\right\} \qquad (29)$$

$$p = 0, 1, \ldots, M \times n - 1, j = 1, 2, \ldots, n,$$

where $q = 0, 1, \ldots, M - 1$, is the remainder of p/M; $M \geq 2N$; and $C_{jm}(q\Delta t)$ is given by

$$C_{jm}(q\Delta t) = \sum_{l=0}^{M-1} B_{jm}(l\Delta\omega) \exp\left(ilq\frac{2\pi}{M}\right), \qquad (30)$$

where, in the current paper, $B_{jm}(l\Delta\omega)$ is expressed by the following equation:

$$B_{jm}(l\Delta\omega)$$

$$= \begin{cases} 2\sqrt{\Delta\omega} H_{jm}\left(l\Delta\omega + \frac{\Delta\omega}{2}\right) \exp(i\phi_{ml}) & 0 \leq l < N \\ 0 & N \leq l < M. \end{cases} \qquad (31)$$

It can be seen from Eqs. (30) and (31) that $C_{jm}(q\Delta t)$ is the Fourier transformation of $B_{jm}(l\Delta\omega)$ and it can thus be computed with the FFT technique.

5. Numerical example

To illustrate the capability and efficiency of the proposed algorithm, two examples involving simulation of turbulent wind velocity processes are selected: simulation of longitudinal wind velocity fluctuations and simulation of longitudinal and vertical wind fluctuating components on a bridge deck.

5.1. Simulation of longitudinal wind velocity fluctuation

An artificial wind velocity field has been generated for the Runyang bridge deck with a main span of 1490 m, shown in Fig. 1, which is a suspension bridge over the Yangtze River constructed in PR China. Although the proposed algorithm has no restriction on the simulated wind field, the longitudinal wind velocity field on the bridge deck is assumed to be composed of 95 wind velocity waves distributed uniformly along the deck for comparison with the previous method. The main data involved in the wind velocity simulation are as follows.

- Span: $L = 1490$ m
- Height of the deck above ground: $z = 60.0$ m
- Ground roughness: $z_0 = 0.01$ m
- Mean wind velocity on the deck: $U(z) = 40.0$ m/s
- Interval between points: $D = 15.851$ m
- Upper cutoff frequency: $\omega_{up} = 4\pi$ rad/s
- Dividing number of frequency: $N = 2048$
- Time interval: $\Delta t = 0.25$ s
- Period: $T_0 = 97, 280$ s.

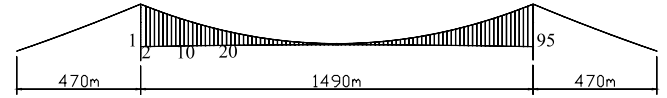Kaimal's two-sided spectrum formula for longitudinal turbulent wind velocity is defined as [19]

Fig. 1. Simulation of longitudinal wind velocity field on the bridge deck.

Table 1
Computing time taken for the three algorithms.

	Deodatis method (original)	Deodatis method (improved)	Proposed algorithm
Computing time	29 min 12 s	20 s	34 s

$$\frac{2nS_u(n)}{u_*^2} = \frac{200f}{(1 + 50f)^{5/3}}, \qquad (32)$$

where

$$f = \frac{nz}{U(z)}, \qquad u_* = \frac{KU(z)}{\ln\left(\frac{z}{z_0}\right)}, \qquad K = 0.4.$$

Davenport's coherence function is computed by

$$\mathrm{coh}_{uu}(r, \omega) = \exp\left(-\frac{\omega}{2\pi}\frac{C_y^{uu}|y_1 - y_2|}{U(z)}\right) \qquad (33)$$

with C_y^{uu} taken as 10.

Three different ergodic simulating algorithms have used to generate the longitudinal wind velocity on the bridge deck for a comparison of their efficiency: the original Deodatis method, the Deodatis method improved by Cao and Xiang [14], and the proposed algorithm. The comparison of computer time using the three algorithms is given in Table 1, in which the three simulations take advantage of the FFT technique. It is noted that the proposed algorithm is more efficient than the original Deodatis method. The improved Deodatis method is the most efficient, but it has a severe restriction on the simulated wind field. However, the proposed algorithm is suitable for the simulation of a general wind velocity field with arbitrary wind spectra on spatial points.

Fig. 2 shows the first 2000 s samples of simulated wind velocities at points 1, 2, 20. It can be seen that the wind velocities at points 1 and 2 have a quite strong correlation between them, since they are close to each other. However, there is a considerable loss of coherence between the wind velocities of points 1 and 20, since the two points are 300 m more apart.

Using the proposed scheme, the temporal and target auto-/cross-correlation functions of simulated wind velocities at some typical points are shown as Fig. 3. It appears that the temporal auto-/cross-correlation functions of simulated wind velocities have good agreement with the target. Hence, this proposed simulation result might be considered satisfactory.

5.2. Simulation of longitudinal and vertical wind fluctuating components

The cross spectra between the longitudinal and vertical wind fluctuations might be not negligible in the buffeting analysis of long-span bridges [20]. Preliminary studies by Ding et al. [21] demonstrated a 18.7% underestimate in buffeting responses for a suspension bridge as a result of neglecting the wind cross spectrum in one instance. Therefore, the simulation of longitudinal and vertical wind fluctuating components is required for the time-domain buffeting analysis of long-span bridges involving the cross-spectrum effects of the wind components.

The two-sided wind spectra of longitudinal and vertical fluctuations can be estimated by the formulae [19]
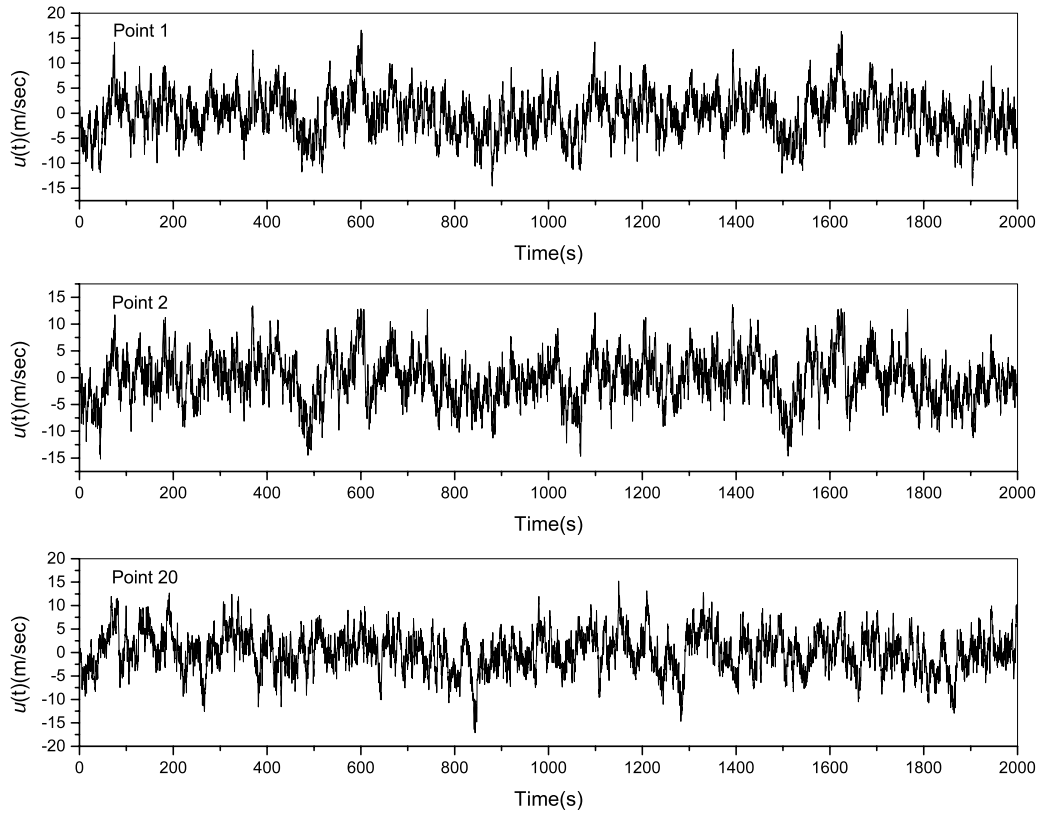
Fig. 2. Samples of simulated wind fluctuations at points 1, 2, 20 ($U = 40$ m/s).
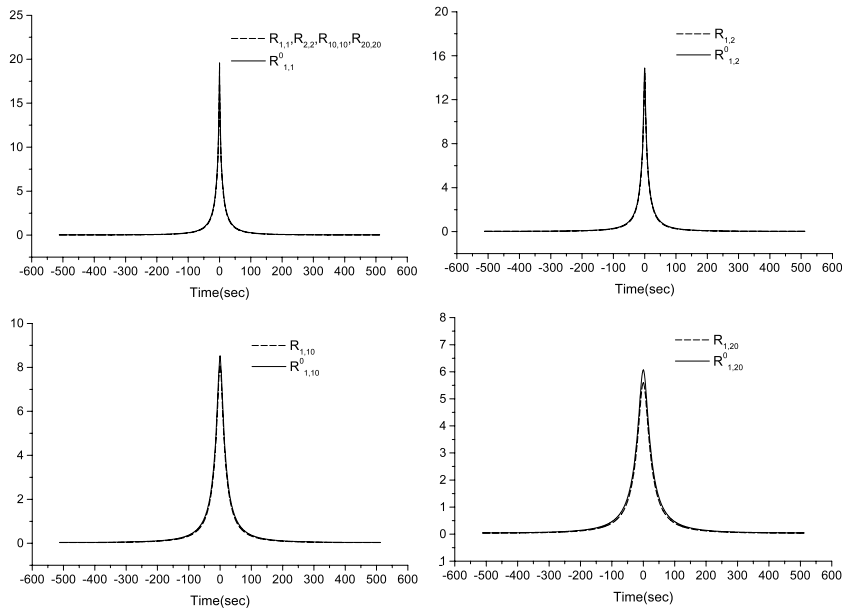

Fig. 3. Correlation functions of simulated wind velocities at points 1, 2, 10, 20.

$$\frac{2nS_u(n)}{u_*^2} = \frac{200f}{(1+50f)^{5/3}} \tag{34}$$

$$\frac{2nS_w(n)}{u_*^2} = \frac{3.36f}{1+10f^{5/3}}; \tag{35}$$

the co-spectrum between u and w is suggested as [20]

$$\frac{2nC_{uw}(n)}{u_*^2} = \frac{14f}{(1+9.6f)^{2.4}}; \tag{36}$$

the quadrature spectrum $Q_{uw}(n)$ is neglected because of lack of

information. The cross-spectral densities of wind fluctuations are expressed in the convention form as

$$S(r,\omega) = \sqrt{S(z_A,\omega)S(z_B,\omega)}\,\text{coh}(r,\omega), \tag{37}$$

where r denotes the distance between two points. For convenience of illustration, the coherence functions of the cross spectrum of wind fluctuations are taken as

$$\text{coh}_{uu}(r,\omega) = \exp\left(-\frac{\omega}{2\pi}\frac{C_y^{uu}|y_1-y_2|}{U(z)}\right) \tag{38}$$
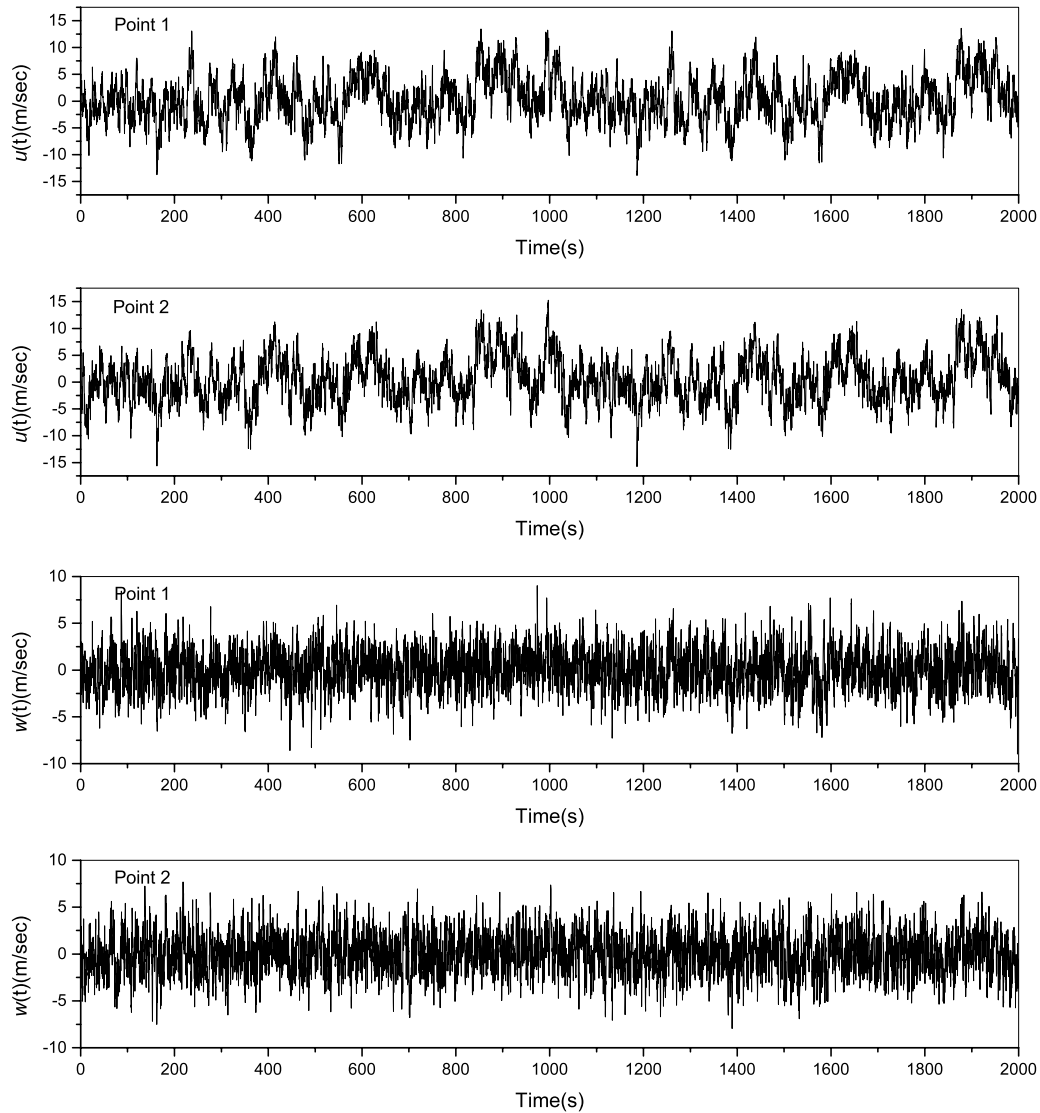
Fig. 4. Samples of simulated wind fluctuations at points 1, 2 ($U = 40$ m/s).

$$\text{coh}_{ww}(r, \omega) = \exp\left(-\frac{\omega}{2\pi}\frac{C_y^{ww}|y_1 - y_2|}{U(z)}\right) \tag{39}$$

$$\text{coh}_{uw}(r, \omega) = \exp\left(-\frac{\omega}{2\pi}\frac{C_y^{uw}|y_1 - y_2|}{U(z)}\right), \tag{40}$$

and C_y^{uu}, C_y^{ww} and C_y^{uw} are simply set as 10 here.

The longitudinal and vertical wind velocities on the Runyang bridge deck are simulated using the proposed algorithm. The upper cutoff frequency ω_{up} is 4π rad/s, the dividing number of frequency N is 2048, and the other parameters used in the wind velocity simulation are the same as those used in the first numerical example. The generation of the 190 wind velocities (95 longitudinal and 95 vertical) takes only 2 m 40 s on a Pentium-IV personal computer and requires about 150 MB computer memory. Since the wind spectra of the longitudinal and vertical wind velocities are not identical, the method proposed by Cao [14] does not work. Use of the existing Deodatis method is prohibitive because of the computer memory requirement.

Fig. 4 shows the first 2000 s samples of simulated longitudinal and vertical wind velocities at points 1 and 2. It is noted that there is a remarkable difference between the longitudinal and vertical wind fluctuations. The longitudinal wind velocities have more

components in the low frequency range than the vertical ones, and there are various maxima for the longitudinal and vertical wind velocities due to the difference of wind spectra.

The temporal and target auto-/cross-correlation functions of simulated wind velocities at points 1 and 2 are shown in Fig. 5. It can be seen that there are good agreements between the temporal and target auto-/cross-correlation functions of simulated wind velocities.

6. Conclusions

A simulation formula to generate stationary multivariate stochastic processes is derived from the Fourier–Stieltjes integral of spectral representation. The proposed algorithm generates ergodic sample functions in the sense that the temporal mean value and temporal auto-/cross-correlation function of any sample function are identical to the corresponding ensemble parts, when the sample length is equal to one period. The algorithm is very efficient computationally since it drastically reduces the computation requirements for Cholesky decomposition and takes advantage of the fast Fourier transform technique. The proposed algorithm can be used for the simulation of stochastic wind velocity processes on bridge decks.
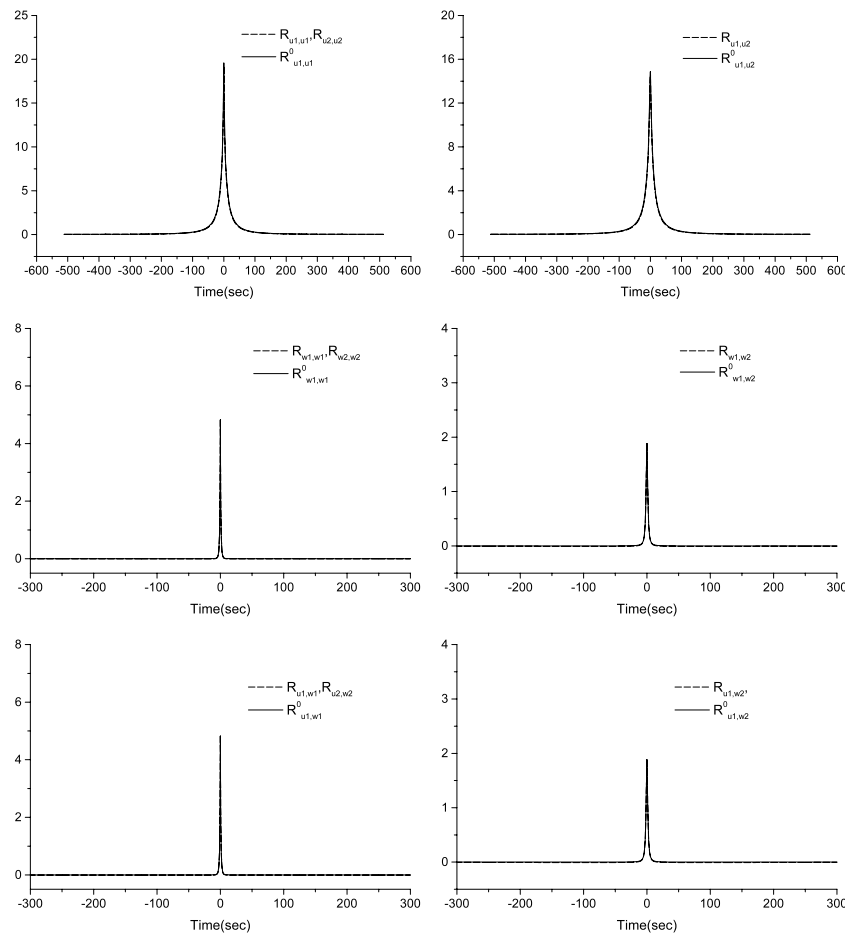
Fig. 5. Correlation functions of simulated wind velocities at points 1, 2.

To illustrate the capability and efficiency of the proposed algorithm, two examples involving simulation of turbulent wind velocity processes were selected. The first example is the simulation of longitudinal wind velocity fluctuations on the deck of the Runyang suspension bridge. It is noted that the proposed algorithm is very efficient and suitable for the simulation of a general wind velocity field with arbitrary wind spectra on spatial points. It appears that the temporal auto-/cross-correlation functions of simulated wind velocities are in good agreement with the target.

The second example is the simulation of longitudinal and vertical wind fluctuating components, which is required for the time-domain buffeting analysis of long-span bridges involving the cross-spectrum effects of the wind components. It can be seen that there are good agreements between the temporal and target auto-/cross-correlation functions of the simulated wind velocities. Hence, this proposed simulation result might be considered satisfactory.

Acknowledgements

References

[1] Spanos PD, Zeldin BA. Monte Carlo treatment of random fields: a broad perspective. Appl Mech Rev 1998;51(3):219–37.
[2] Shinozuka M. Simulation of multivariate and multidimensional random processes. J Acoust Soc Am 1971;49:357–68.
[3] Shinozuka M, Jan CM. Digital simulation of random processes and its applications. J Sound Vib 1972;25(10):111–28.
[4] Yang J. Simulation of random envelope processes. J Sound Vib 1972;21(1):73–85.
[5] Shinozuka M. Digital simulation of random processes in engineering mechanics with the aid of FFT technique. In: Ariaratnam ST, Leipholz HHE, editors. Stochastic problems in mechanics. Ontario (Canada): University of Waterloo Press; 1974. p. 277–86.
[6] Deodatis G. Simulation of ergodic multivariate stochastic processes. J Eng Mech, ASCE 1996;122(8):778–87.
[7] Shinozuka M. Stochastic fields and their digital simulation. In: Schuëller GI, Shinozuka M, editors. Stochastic methods in structural dynamics. Dordrecht (The Netherlands): Martinus Nijhoff Publishers; 1987. p. 93–133.
[8] Shinozuka M, Deodatis G. Simulation of stochastic processes by spectral representation. Appl Mech Rev 1991;44(4):191–204.
[9] Shinozuka M, Yun CB, Seya H. Stochastic methods in wind engineering. J Wind Eng Ind Aerodyn 1990;36:829–43.
[10] Kovacs I, Svensson HS, Jordet E. Analytical aerodynamic investigation of cable-stayed Helgeland bridge. J Struct Eng, ASCE 1992;118(1):147–68.
[11] Mann J. Wind field simulation. Probab Eng Mech 1998;13:269–82.
[12] Di Paola M. Digital simulation of wind field velocity. J Wind Eng Ind Aerodyn 1998;74–76:91–109.
[13] Yang WW, Chang TYP, Chang CC. An efficient wind field simulation technique for bridges. J Wind Eng Ind Aerodyn 1997;67–68:697–708.
[14] Cao YH, Xiang HF, Zhou Y. Simulation of stochastic wind velocity field on long-span bridges. J Eng Mech, ASCE 2000;126(1):1–6.
[15] Li Y, Kareem A. Simulation of multivariate random processes: hybrid DFT and digital filtering approach. J Eng Mech, ASCE 1993;119(5):1078–98.
[16] Solari G, Carassale L. Modal transformation tools in structural dynamics and wind engineering. Wind Struct 2000;3(4):221–41.
[17] Grigoriu M. A spectral representation based model for Monte Carlo simulation. Probab Eng Mech 2000;15:365–70.
[18] Priestley MB. Spectral analysis and time series. San Deiego (CA): Academic; 1981.
[19] Simiu E, Scanlan RH. Wind effects on structures. New York: Wiley; 1986.
[20] Jones NP, Jain A, Scanlan RH. Wind cross-spectrum effects on long-span bridges. In: Proceedings of engrg. mech. spec. conf. ASCE. New York. 1992.
[21] Ding QS, Chen AR, Xiang HF. Coupled buffeting response analysis of long-span bridges by the CQC approach. Struct Eng Mech 2002;14(5):505–20.